Atmospheric Refractivity Tracking From Radar Clutter Using Kalman and Particle Filters

Caglar Yardim, Peter Gerstoft, William S. Hodgkiss
University of California, San Diego
La Jolla, CA 92093–0238, USA
email: cyardim@ucsd.edu, gerstoft@ucsd.edu, whodgkiss@ucsd.edu

***Abstract*— This paper addresses the problem of tracking the spatial and temporal lower atmospheric variations in marine and coastal environments. The method tracks the evolution of the range and height-dependent index of refraction using the sea clutter measured from sea-borne radars operating in the region. A split-step fast Fourier transform based parabolic equation approximation to the wave equation is used to compute the clutter return in complex environments with varying index of refraction. In addition, regional statistics are incorporated as prior densities, resulting in a highly nonlinear and non-Gaussian tracking problem. Various tracking algorithms such as the extended Kalman, unscented Kalman and particle filters are used for tracking surface-based electromagnetic ducts frequently encountered in marine environments. Tracking performance of each filter is also calculated and compared using the posterior Cramér-Rao lower bound. Even though the tracking performance of the Kalman filters was limited by the high non-linearity of the parabolic equation, particle filters proved to be very promising in tracking even the abruptly changing environments.**

I. Introduction

In many maritime regions of the world, such as the Mediterranean, Persian Gulf, East China Sea, and California Coast, atmospheric ducts are common occurrences. They result in various anomalies such as significant variations in the maximum operational radar range and increased sea clutter. Therefore, it is important to predict the real-time 3-D environment (characterized by the modified refractivity profile, M-profile) the radar is operating in so that the radar operator will at least know the true system limitations and in some cases even compensate for them. Some of the conventional techniques that measure or predict the lower atmospheric index of refraction include radiosondes and rocketsondes, microwave refractometers, meteorological models such as the Coupled Ocean/Atmospheric Mesoscale Prediction System (COAMPS), lidar and GPS measurements.

However, it is also possible to predict the duct properties using the radar itself. When launched at a low elevation angle, the electromagnetic signal will be trapped within the duct which can be taken as a range-dependent leaky waveguide bounded from below by the sea surface. This will result in multiple reflections and strong interaction with the surface which in turn will result in an increase in the sea clutter, forming clutter rings. This normally unwanted portion of the received signal can then be used to infer the environment that would give such a clutter structure. These techniques can be classified as refractivity-from-clutter (RFC) techniques [1]–[4]. Other RFC techniques and more detailed discussions about the differences between them can be found in [4].

This paper is a natural extension to these previous RFC methods which compute the 2-D range and height-dependent M-profile for a given azimuth direction. Instead of inverting the environmental parameters for a given azimuth and time, the emphasis is on tracking both the temporal and spatial evolutions of duct parameters. Throughout this paper, the term spatial evolution will be used to represent the evolution of the 2-D M-profile with the rotating azimuth angle of the radar. This is achieved by employing various tracking filters. The problem is formulated in a Kalman framework, where the clutter for a given environment is calculated using a split-step fast Fourier transform (FFT) based parabolic equation (PE) approximation to the wave equation [5]. This introduces a high level of nonlinearity in the measurement equation. The problem is then solved by using various tracking algorithms.

II. Theory

Two equations are necessary to fully characterize the dynamic system; one that describes the evolution of the lower atmosphere and another that governs the propagation of the electromagnetic signal in this environment. At a time step k, these equation can be given as:

$$\mathbf{x}_k = \mathbf{F}\mathbf{x}_{k-1} + \mathbf{v}_{k-1} \tag{1}$$

$$\mathbf{y}_k = \mathbf{h}\left(\mathbf{x}_k\right) + \mathbf{w}_k \tag{2}$$

where $\mathbf{F}$ is a known linear function of the state vector $\mathbf{x}_k$, $\mathbf{h}(\cdot)$ is a known nonlinear function of the measurement vector $\mathbf{y}_k$, $\mathbf{v}_k$ and $\mathbf{w}_k$ are the process and the measurement noise vectors, respectively with

$$\begin{aligned} &\mathrm{E}\{\mathbf{v}_k\mathbf{v}_i^{\mathrm{T}}\} = \mathbf{Q}_k\delta_{ki} \qquad \mathrm{E}\{\mathbf{w}_k\mathbf{w}_i^{\mathrm{T}}\} = \mathbf{R}_k\delta_{ki} \\ &\mathrm{E}\{\mathbf{v}_k\mathbf{w}_i^{\mathrm{T}}\} = \mathbf{0} \quad \forall\, i,k. \end{aligned} \tag{3}$$

The state vector $\mathbf{x}_k$ is composed of the n_x parameters that describe the complex environment at the step index k. The state vector for the surface-based duct (SBD) is given in Appendix I. The process noise $\mathbf{v}_k$ is a zero-mean additive Gaussian probability density function (pdf). Prior density $\mathrm{p}(\mathbf{x}_o)$ is usually constructed using the regional statistics. This density must be Gaussian for the Kalman filters but it can be any distribution for the particle filter.

Equation (1) is the state equation for the stochastic environmental model. $\mathbf{F}$ is the linear state transition matrix which will be taken as the identity matrix. The main assumption is that the environment is changing slowly compared to the step index. Although the M-profile is not expected to vary considerably in short intervals, sudden fluctuations can occur and the filters will require larger $\mathbf{Q}_k$ to perform adequately in these environments. From many previous experiments such as the Variability of Coastal Atmospheric Refractivity (VOCAR) [6], it is known that spatial and temporal duct variability are strong functions of region, season, time of the day and mesoscale atmospheric processes. For example, experiments indicate that Santa Ana-induced (warm and dry offshore winds in Southern and Baja California) SBDs typically have higher spatial variability than the subsidence-induced SBDs [7]. The duct parameters such as the duct height have also been observed to stay stable for days, followed by rapid fluctuations [8]. Spatial variability also has similarly challenging and dynamic patterns as shown during the Wallops'2000 experiment [9]. Hence, different environmental models may be necessary for different applications or regions.

Equation (2) is the measurement equation and it relates the environment given by $\mathbf{x}_k$ to the radar clutter power $\mathbf{y}_k$ through a highly nonlinear $\mathbf{h}(\cdot)$ function which uses a split-step FFT-PE (see Appendix II). The degree of nonlinearity and hence the filter performance heavily depends on the current location of $\mathbf{x}_k$ on the state-space. As stated in Appendix II, $\mathbf{w}_k$ is the logarithm of the sea surface clutter radar cross section (RCS). There are many successful models for the sea clutter distribution. The selection of the appropriate model depends on various factors such as the grazing angle, radar resolution and sea roughness. Some of the commonly used models include the Rayleigh, Weibull, log-normal and K-distributed sea clutter [10], [11]. Since the Kalman framework requires Gaussian distributions, the model can only be constructed if RCS is selected as log-normal even if this may not be the most suitable selection among the densities mentioned above. The PF does not have such restrictions and any pdf can be used. Since it is desirable to compare these filters under the same set of assumptions, sea clutter is taken as log-normal.

A. Tracking Algorithms

Since the tracking problem given in (1)–(2) is nonlinear with non-Gaussian densities, a Kalman filter (KF) cannot be used. Instead, an extended Kalman filter (EKF) [12] is used by locally linearizing the equations using the first terms in the Taylor series expansions (Jacobian) of the nonlinear transformations (such as $\mathbf{h}$) and hoping that the nonlinearities are mild enough that EKF will still perform well. Since the pdfs are Gaussian and equations are linearized, it is necessary to propagate only the mean and covariance as in KF. However due to this approximation, the EKF cannot claim the optimality enjoyed by the KF for linear-Gaussian systems. The EKF has been successfully implemented in a large number of applications such as many radar and sonar target tracking applications and its speed and ease of implementation makes the EKF the filter of choice. Therefore, the EKF is the first filter tested in the RFC tracking problem.

To alleviate some of the problems the EKF is faced with, the unscented Kalman filter (UKF) [13] has been introduced. Unlike the EKF which tackles the problem by enforcing linearity, this filter approaches the problem from a different angle by enforcing Gaussianity and keeping the nonlinearity. This still enables the filter to carry all the necessary information by propagating only the mean and covariance as a KF does. It uses an unscented transformation (UT) that enables the propagation of the mean and variance through nonlinear functions. The UKF represents initial densities using only a few predetermined particles called the sigma points. These particles are chosen deterministically by the UT algorithm and they can describe accurately the mean and covariance of a pdf. As the random variable undergoes a nonlinear transformation, these particles are propagated through this nonlinear function and used to reconstruct the new mean and covariance using the UT weights. Hence, unlike the EKF, they can compute accurately the mean and covariance to at least second order (third if the initial density is Gaussian) of the nonlinearity. It is a fast, derivative-free algorithm but UKF may still perform poorly in a highly nonlinear or non-Gaussian system.

The last algorithm analyzed in this paper is the particle filter (PF) [14] which is used for many nonlinear, non-Gaussian tracking problems. The main difference with Kalman type filters is that, since no Gaussian assumption is made, propagating the mean and covariance will not be sufficient. Instead the PF will propagate particles to represent the densities just as in the UKF; with notable differences. The first is that the particles in the PF will be selected randomly by MC runs and typically a much larger number of particles will be needed to represent the pdf. Therefore, the PF can perform much better than its KF variants but it does this with an order of magnitude increase in the computational burden.

B. Posterior Cramér-Rao Lower Bound

It is usually not possible to have an optimal estimator to nonlinear filtering problems such as the RFC. All the techniques used in this paper are also sub-optimal techniques. Therefore, it is desirable to have a tool that can not only assess the performances of these sub-optimal techniques but also provide a limit to achievable performance for a given environment.

In a classical non-Bayesian framework, the Cramér-Rao Lower Bound (CRLB), which is the inverse of the Fisher information matrix (FIM), is commonly used. For a Bayesian framework this instead can be replaced by the posterior Cramér-Rao Lower Bound (PCRLB) introduced by van Trees [15]. Since this paper exclusively deals with PCRLB, it will henceforth be referred simply as CRLB.

Any filter that can lower its mean square error to the CRLB is called an efficient estimator. For a linear and Gaussian system, the Kalman filter is an efficient estimator. It may not be possible to attain the CRLB for a nonlinear, non-Gaussian system.

Let $\mathbf{J}_k$ be the inverse of the CRLB$_k$ as a $(n_x \times n_x)$ filtering information matrix so that the mean-square error of any filter estimate at tracking step index k will be bounded as

$$\mathrm{E}\left\{\left(\widehat{\mathbf{x}}_{k|k}-\mathbf{x}_k\right)\left(\widehat{\mathbf{x}}_{k|k}-\mathbf{x}_k\right)^{\mathrm{T}}\right\} \geq \mathbf{J}_k^{-1}, \tag{4}$$

where $\widehat{\mathbf{x}}_{k|k}$ is the estimate of $\mathbf{x}_k$ given its previous history $\{\mathbf{x}_o, \mathbf{x}_1, \ldots, \mathbf{x}_{k-1}\}$ and the set of measurements $\{\mathbf{y}_1, \mathbf{y}_2, \ldots, \mathbf{y}_k\}$. A computationally efficient way of computing this CRLB recursively for discrete-time nonlinear filtering problems is proposed in [16]:

$$\mathbf{J}_k = \mathbf{D}_{k-1}^{22} - \left[\mathbf{D}_{k-1}^{12}\right]^{\mathrm{T}}\left(\mathbf{J}_{k-1}+\mathbf{D}_{k-1}^{11}\right)^{-1}\mathbf{D}_{k-1}^{12} \tag{5}$$

where

$$\mathbf{D}_{k-1}^{11} = -\mathrm{E}\left\{\nabla_{\mathbf{x}_{k-1}}\left[\nabla_{\mathbf{x}_{k-1}}\log \mathrm{p}\left(\mathbf{x}_k|\mathbf{x}_{k-1}\right)\right]^{\mathrm{T}}\right\} \tag{6}$$

$$\mathbf{D}_{k-1}^{12} = -\mathrm{E}\left\{\nabla_{\mathbf{x}_k}\left[\nabla_{\mathbf{x}_{k-1}}\log \mathrm{p}\left(\mathbf{x}_k|\mathbf{x}_{k-1}\right)\right]^{\mathrm{T}}\right\} \tag{7}$$

$$\begin{aligned}\mathbf{D}_{k-1}^{22} = &-\mathrm{E}\left\{\nabla_{\mathbf{x}_k}\left[\nabla_{\mathbf{x}_k}\log \mathrm{p}\left(\mathbf{x}_k|\mathbf{x}_{k-1}\right)\right]^{\mathrm{T}}\right\} \\ &-\mathrm{E}\left\{\nabla_{\mathbf{x}_k}\left[\nabla_{\mathbf{x}_k}\log \mathrm{p}\left(\mathbf{y}_k|\mathbf{x}_k\right)\right]^{\mathrm{T}}\right\}.\end{aligned} \tag{8}$$

Note that the computations only require $(n_x \times n_x)$ matrices and the computational cost is independent of the step index k.

Taking into account that the system defined in (1) – (2) has a linear state equation and both of the random noise sequences **v** and **w** are additive and Gaussian, the above equations will be reduced to

$$\begin{aligned}&\mathbf{D}_{k-1}^{11} = \mathbf{F}^{\mathrm{T}}\mathbf{Q}^{-1}\mathbf{F} \qquad \mathbf{D}_{k-1}^{12} = -\mathbf{F}^{\mathrm{T}}\mathbf{Q}^{-1} \\ &\mathbf{D}_{k-1}^{22} = \mathbf{Q}^{-1} + \mathrm{E}\left\{\mathbf{H}_k^{\mathrm{T}}\mathbf{R}_k^{-1}\mathbf{H}_k\right\},\end{aligned} \tag{9}$$

where

$$\mathbf{H}_k = \left[\nabla_{\mathbf{x}_k}\mathbf{h}^{\mathrm{T}}\left(\mathbf{x}_k\right)\right]^{\mathrm{T}} \tag{10}$$

is the Jacobian of $\mathbf{h}(\mathbf{x})$ evaluated at its true value $\mathbf{x}_k$. Unfortunately the expectation in (9) has to be evaluated numerically. The recursion is initiated by using the prior to compute $\mathbf{J}_o$ as

$$\mathbf{J}_o = -\mathrm{E}\left\{\nabla_{\mathbf{x}_o}\left[\nabla_{\mathbf{x}_o}\log \mathrm{p}\left(\mathbf{x}_o\right)\right]^{\mathrm{T}}\right\} = \mathbf{P}_o^{-1}. \tag{11}$$

III. Examples

This section is composed of two examples covering the temporal tracking of surface-based ducts. Throughout the examples issues such as the performance limitations, filter efficiencies, divergence characteristics, and CPU time comparisons are addressed.

A. Case Study I: Temporal Tracking of a Range-Independent Surface-Based Duct

This example is used to compare the tracking performances of the EKF, UKF and PF and compute their efficiencies using the numerically computed CRLB. The range-independent SBD is selected from the environmental library (previously known as the Ducting Climatology Summary (DCS) database) of the Advanced Refractive Effect Prediction System (AREPS) [17]. The Bahrain radiosonde station in the Persian Gulf is used for the simulation (Fig. 1). The station, average environment, radar and simulation parameters are given in Table I, where the layer thicknesses and slopes are defines as in Appendix I. The fact that only SBD (excluding evaporative and elevated ducts) is present an average of 67% of the time clearly makes estimation and tracking of atmospheric ducts a high priority in Persian Gulf and many other regions of the world. The same frequency as that of the Space Range Radar (SPANDAR) employed in the Wallops island experiments [1], [9] is used. The height is set to 15 m, a typical value for a naval radar.

TABLE I

Case Study I: Comparison of Tracking Algorithms and CRLB

Radiosonde Station Bahrain, Persian Gulf

Station		**Environment**	
Longitude	50°36′E	Duct Type	Surface-based duct
Latitude	26°18′N	Month	Mar/Apr/May average
Elevation	2 m	Time	Day/night average
Marsden Square	103	Occurrence	59% day / 75% night
Radar		c_1	0.500 M-units/m
Frequency	2.84 GHz	c_2	-0.221 M-units/m
Altitude	15 m	h_1, h_2	43 m, 77 m
Simulation Parameters			
Monte Carlo runs	100		
Track length	30 min – 1 measurement/min		
Initial covariance	$\mathbf{P}_o$ = diag[0.01^2, 0.01^2, 3^2, 3^2]		
State noise covariance	$\mathbf{Q}$ = diag[0.003^2, 0.003^2, 1^2, 1^2]		
Measurement noise	log–normal, $\mathbf{R}$ = diag[5^2 dB^2]		

The CRLB is calculated using Monte Carlo analysis. 100 environmental parameter trajectories are created from the state equation (1) with starting values randomly selected from the prior density. $\mathbf{D}_{k-1}^{22}$ is then calculated using

$$\mathbf{D}_{k-1}^{22} = \mathbf{Q}^{-1} + \frac{1}{N_{MC}}\sum_{j=1}^{N_{MC}}\nabla\mathbf{h}\left(\mathbf{x}_{k-1}^{j}\right)\mathbf{R}^{-1}\left[\nabla\mathbf{h}\left(\mathbf{x}_{k-1}^{j}\right)\right]^{\mathrm{T}}. \tag{12}$$

Each of these environments is also tracked using the EKF, UKF and PF. The results are given in Fig. 1 and Table II. The performance metrics are defined as follows:

$$\eta_k(i) = \mathbf{J}_k^{-1/2}(i,i) \;/\; \mathrm{RMS}_k(i) \tag{13}$$

$$\mathrm{RTAMS}(i) = \left[\sum_{k=k_1}^{k_2}\sum_{j=1}^{N_{MC}}\frac{\left(\widehat{\mathbf{x}}_k^j(i)-\mathbf{x}_k^j(i)\right)^2}{(k_2-k_1+1)N_{MC}}\right]^{1/2} \tag{14}$$

$$Improv. = \frac{RTAMS_{EKF} - RTAMS_{filter}}{RTAMS_{EKF}} \tag{15}$$

where $\mathbf{x}_k^j(i)$ is the ith parameter of the true state vector $\mathbf{x}$ at time index k for the jth MC run, RMS$_k$ and η_k are the root mean square error and the filter efficiency at step k, RTAMS is the root time averaged mean square error [14] calculated for the interval [k_1,k_2], and (15) is used to calculate the performance improvement of a filter with respect to the EKF. RTAMS is calculated for the 5-30 min. interval so that the initial variation will not affect the performance calculations.

TABLE II

PERFORMANCE COMPARISON FOR CASE STUDY I

Method	RMS Error After 30 min.						RTAMS				Average % Improvement Over EKF
	c_1	c_2	h_1	h_2	Avg. Error	Average	c_1	c_2	h_1	h_2	
	(M-units/km)		(m)		(%)	η (%)	(M-units/km)		(m)		
EKF	12.7	20.5	3.36	11.01	14.2	8	11.7	18.8	3.03	9.48	-
UKF	8.5	16.0	2.33	7.64	9.9	12	6.5	11.9	1.87	6.98	36
PF−200	5.5	2.6	0.71	3.72	4.7	30	4.9	2.7	0.73	3.50	71
PF−1000	3.1	1.9	0.38	0.97	2.3	58	3.6	2.2	0.59	1.96	79
PF−5000	2.0	1.7	0.23	0.96	1.6	77	2.9	2.2	0.46	1.20	84
$\sqrt{\mathbf{CRLB}}$	2.0	1.0	0.21	0.57	1.4	100	2.1	1.0	0.24	0.67	90

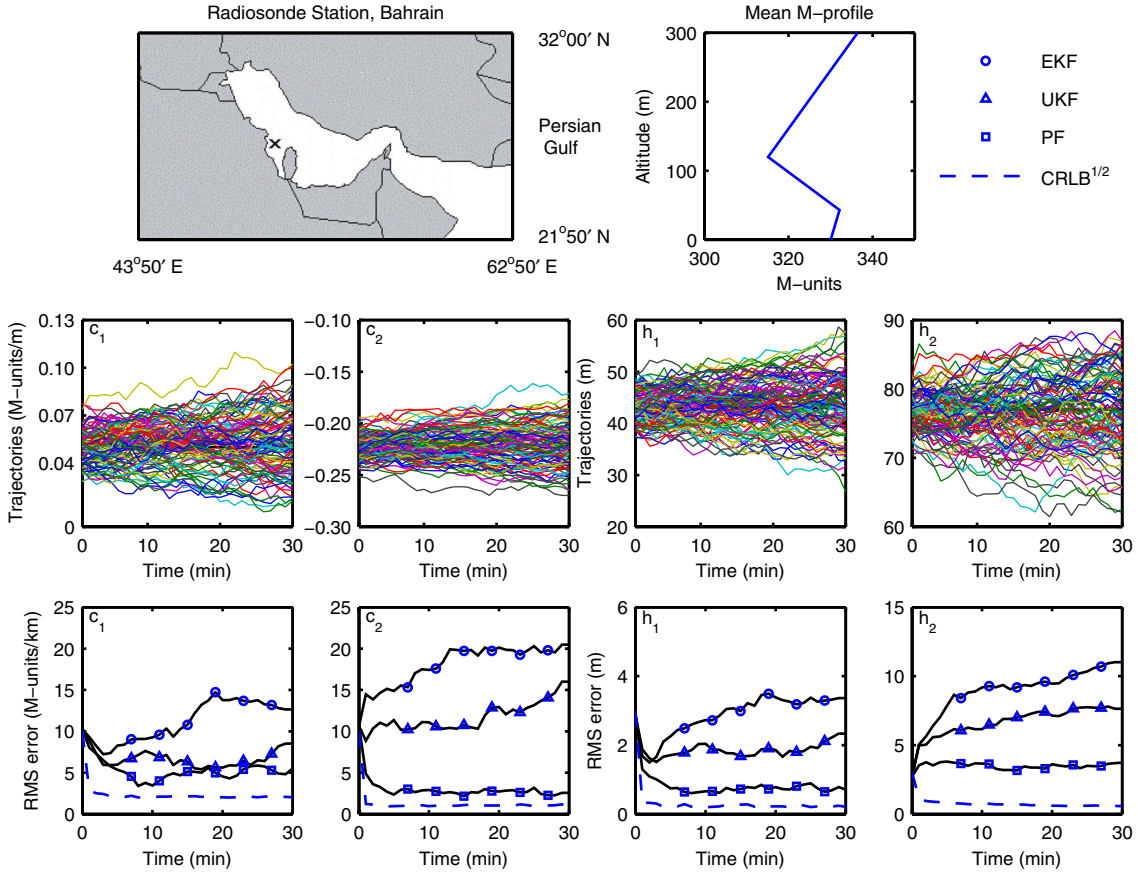

Fig. 1. Case study I for comparison of the tracking algorithms. Location of the station (×), average spring M-profile, evolution of 100 Monte Carlo trajectories, RMS errors of the EKF (O), UKF (△), and 200-particle PF (□) obtained from the tracking performance of these trajectories along with the square root of the posterior CRLB (dashed).

The results in Fig. 1 show that Kalman filters suffer due to their inherent approximations. The measurement equation is highly nonlinear for most of the state space and linearization using the Jacobian clearly does not work for this scenario. Since the UKF does not assume linearity its enjoys an average of 36% improvement over the EKF results. However, a pure Gaussian assumption and high nonlinearity also results in poor UKF estimates with only 12% efficiency. All the particle filters used in this case perform better than both of the Kalman filters. The PF with 5000 particles has an average error of only 1.6%, very close to the value of 1.4% predicted by the CRLB. It is 77% efficient and enjoys a 84% improvement over the EKF. However, it should be noted that PF requires orders of magnitude more of CPU time. The PF-200 required a factor of 10 more CPU time than that of the UKF for this scenario. Hence, the PF is a costly alternative and as a general rule should be avoided as long as the Kalman frameworks provide reasonable tracking.

Atmospheric parameters can sometimes fluctuate abruptly. This requires increasing $\mathbf{Q}_k$ to compensate for the sudden

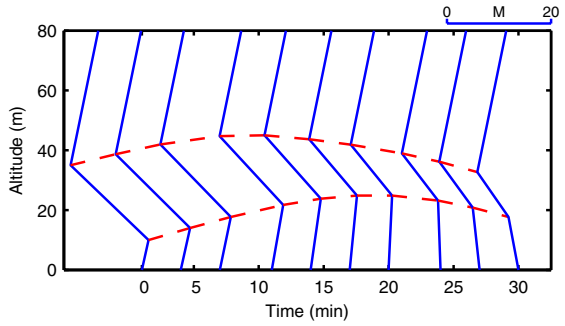

Fig. 2. Case Study II: Temporal evolution of the range-independent duct.

jumps. Initial tests showed that the Kalman structures are very sensitive to these sudden moves and diverge if the sudden jump is large enough, even after $\mathbf{Q}_k$ is increased, whereas particle filters showed robust tracking performance. Therefore, as a general conclusion it can be said that SBD tracking requires particle filters even though they are computationally expensive.

B. Case Study II: Divergence in Surface-Based Duct Tracking

This example studies the divergence problem in SBD tracking using a deterministic trajectory. The height and slope values (Fig. 2) and their variations are selected similar to the helicopter measured real M-profiles obtained in the Wallops island'98 experiment [1]. All the radar and simulation parameters are kept the same as Case Study I except $\mathbf{Q}$ for the layer slopes and sea surface RCS variance are taken as 10^{-4} M-units^2/m^2 and 16 dB^2, respectively. This fixed trajectory is tracked 100 times by each filter to obtain divergent track probabilities.

The evolution of the clutter signal without the addition of noise is given in Fig. 3. This strong nonlinearity of $\mathbf{h}(\mathbf{x}_k)$ results in a high percentage of track divergence for the Kalman filters. For this scenario, a track is declared as divergent if any of the slope estimates for c_1 or c_2 has a RMS error greater than 50 M-units/km or any of the layer thickness estimates for h_1 or h_2 has a RMS error larger than 5 m for any 5 consecutive minutes. A typical track result is given in Fig. 4 for each filter type. The divergence statistics of the filters are provided in Table III. Similar to Case Study I, the PF performs significantly better than both Kalman filters and the UKF is more preferable to the EKF. Actually both Kalman filters were mostly able to follow the thickness variations but failed in tracking the slopes which usually have more effect on the clutter return. Interestingly the EKF RTAMS error for the layer thickness is less than that of the UKF. However, this is more than offset by the fact that after only 10 min, the EKF reached a 47% divergence rate while none of the UKF runs diverged. The PF-200 starts to diverge after 30 min. with a 17% rate and only 1% of the PF-1000 runs failed to track the duct after 30 min.

IV. Conclusion

The extended and unscented Kalman and particle filters are used for tracking the spatial and temporal evolutions of the

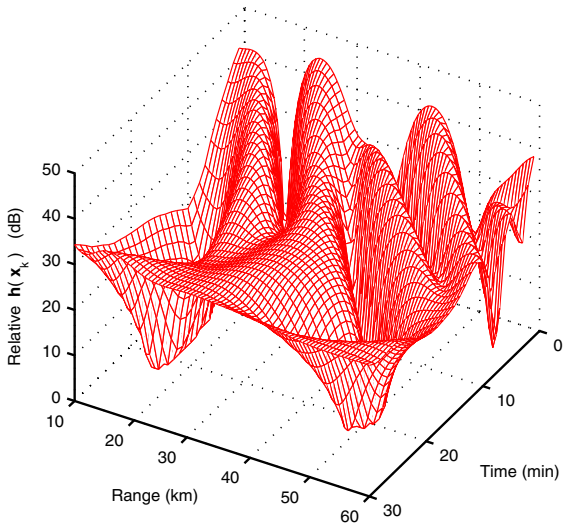

Fig. 3. Evolution of the highly nonlinear relative radar clutter $\mathbf{y}_k$ computed for the true environment without $\mathbf{w}_k$.

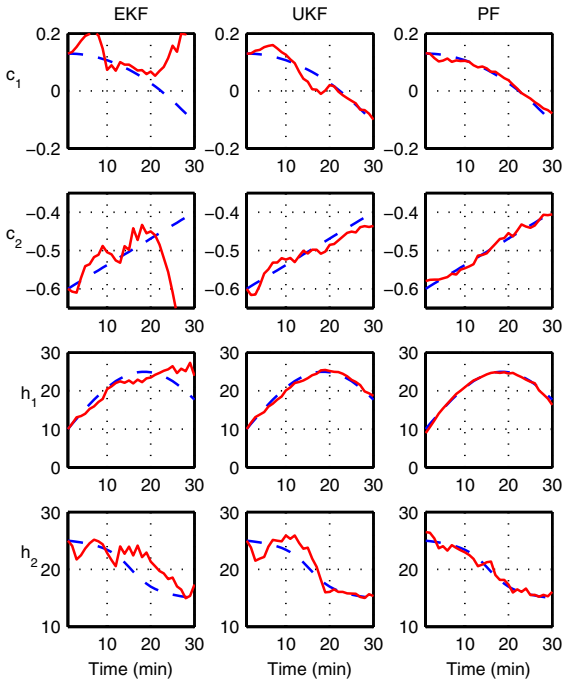

Fig. 4. Case Study II: Temporal tracking of the range-independent SBD. c_1 and c_2 are in M-units/m and h_1 and h_2 are in meters. True trajectories (dashed) and filter estimates (solid) for the EKF, UKF and PF-200.

TABLE III
PERFORMANCE COMPARISON FOR CASE STUDY II

Method	Average RTAMS		Divergent Track Percentage After		
	M-units/km	m	10 min.	20 min.	30 min.
EKF	84.2	2.9	47	69	90
UKF	41.8	3.3	0	29	37
PF−200	27.7	0.9	0	0	17
PF−1000	16.2	0.5	0	0	1

lower atmosphere using radar clutter. The divergence statistics, computational complexities, and tracking performances of these filters are compared to each other using the posterior CRLB.

V. Acknowledgment

This work was supported by the Office of Naval Research under grant N00014-05-1-0369.

Appendix I
Creation of the 2-D Modified Refractivity Profile from State Variables

Surface-based ducts (SBD) are represented by the commonly used tri-linear M-profiles. Each tri-linear profile requires four parameters: slope and thickness of the base (c_1, h_1) and inversion layers (c_2, h_2). The top layer slope is taken to be constant at 0.118 M-units/m. For range-dependent profiles, the M-profile parameters are defined at n_r range intervals and the values at other ranges are calculated using a cubic fit. Hence, the number of state parameters $n_x = 4n_r$. The 2-D M-profile is calculated using the following procedure:

$$\mathbf{x}_k = \left[\mathbf{m}_1^{\mathrm{T}}\ \mathbf{m}_2^{\mathrm{T}}\ \ldots\ \mathbf{m}_{n_r}^{\mathrm{T}}\right]^{\mathrm{T}} \tag{16}$$

$$\mathbf{m}_i = \left[c_1(r_i)\ c_2(r_i)\ h_1(r_i)\ h_2(r_i)\right]^{\mathrm{T}} \quad i = 1, \ldots, n_r \tag{17}$$

$$M(z,r) = M_0 + \begin{cases} \tilde{c}_1 z & \text{if } z \le \tilde{h}_1 \\ \tilde{c}_1\tilde{h}_1 + \tilde{c}_2(z-\tilde{h}_1) & \text{if } \tilde{h}_1 \le z \le \tilde{h}_2 \\ \tilde{c}_1\tilde{h}_1 + \tilde{c}_2\tilde{h}_2 & \text{if } z \ge \tilde{h}_2 \\ \quad +0.118(z-\tilde{h}_1-\tilde{h}_2), & \end{cases} \tag{18}$$

where M_0 is the base refractivity usually taken as 330 M-units/m, $\mathbf{m}_i$ represent the trilinear profiles at n_r different ranges defined in the state vector, $\tilde{c}_1$, $\tilde{c}_2$, $\tilde{h}_1$, and $\tilde{h}_2$ are cubic fitted parameters at range r.

Appendix II
Measurement Equation – Propagation Model

The measurement equation provides $\mathbf{y}_k$, the radar clutter power in dB, for an environment described by the state vector $\mathbf{x}_k$. First the field is propagated in range using the following recursive split-step FFT PE formula [18]

$$u_k(z, r+\triangle r) = \exp\left[ik_o \triangle r M(\mathbf{x}_k)10^{-6}\right] \times \mathfrak{F}^{-1}\left\{\exp\left[i\triangle r\left(\sqrt{k_o^2 - k_z^2} - k_o\right)\right]\mathfrak{F}\left\{u_k(z,r)\right\}\right\} \tag{19}$$

where $u_k(z,r)$ is the vertical electromagnetic field at range r at step index k, k_o and k_z are the wavenumber and its vertical component, $\triangle r$ is the range increment in PE, $\mathfrak{F}$ and $\mathfrak{F}^{-1}$ are the Fourier and inverse Fourier transforms and $M(\mathbf{x}_k)$ is the 2-D M-profile $M(z,r)$ computed in Appendix I. Following [1], the clutter power $\mathbf{P_c}$ for low grazing angles can be calculated using

$$\mathbf{P_c} = c\mathbf{L}^{-2}(\mathbf{x}_k) r \sigma^o \tag{20}$$

where c accounts for the constant terms in the radar equation, $\mathbf{L}(\mathbf{x}_k)$ is the one way propagation loss obtained from the electromagnetic field $u_k(z,r)$ calculated at the effective scattering height given as 0.6 times the mean wave height [19] and σ^o is the normalized sea surface RCS.

The measurement equation (2) can be obtained by representing (20) in dB with the following definitions

$$\mathbf{y}_k = 10\log(\mathbf{P_c}) \qquad \mathbf{w}_k = 10\log(\sigma^o) \tag{21}$$

$$\mathbf{h}\left(\mathbf{x}_k\right) = -20\log\mathbf{L}(\mathbf{x}_k) + 10\log(cr) \tag{22}$$

where the measurement noise $\mathbf{w}_k$ is additive Gaussian since σ^o is the sea surface RCS with log-normal pdf.

References

[1] P. Gerstoft, L. T. Rogers, J. Krolik, and W. S. Hodgkiss, "Inversion for refractivity parameters from radar sea clutter," *Radio Science*, vol. 38 (3), pp. 1–22, 2003, doi:10.1029/2002RS002640.

[2] P. Gerstoft, W. S. Hodgkiss, L. T. Rogers, and M. Jablecki, "Probability distribution of low altitude propagation loss from radar sea-clutter data," *Radio Science*, vol. 39, pp. 1–9, 2004, doi:10.1029/2004RS003077.

[3] C. Yardim, P. Gerstoft, and W. S. Hodgkiss, "Estimation of radio refractivity from radar clutter using Bayesian Monte Carlo analysis," *IEEE Trans. Antennas Propagat.*, vol. 54(4), pp. 1318–1327, 2006.

[4] ——, "Statistical maritime radar duct estimation using a hybrid genetic algorithms – Markov chain Monte Carlo method," *Radio Science*, in press.

[5] M. Levy, *Parabolic Equation Methods for Electromagnetic Wave Propagation*. London, United Kingdom: The Institution of Electrical Engineers, 2000.

[6] T. Haack and S. D. Burk, "Summertime marine refractivity conditions along coastal California," *Journal of Applied Meteorology*, vol. 40, pp. 673–687, 2001.

[7] R. A. Paulus, "An overview of an intensive observation period on variability of coastal atmospheric refractivity," in *AGARD/NATO Conference on Propagation Assessment in Coastal Environments*, Bremerhaven, Germany, February, 1995.

[8] I. M. Brooks, A. K. Goroch, and D. P. Rogers, "Observations of strong suface radar ducts over the Persian gulf," *Journal of Applied Meteorology*, vol. 38, pp. 1293–1310, 1999.

[9] J. K. Stapleton, V. R. Wiss, and R. E. Marshall, "Measured anomalous radar propagation and ocean backscatter in the Virginia coastal region," in *31st International Conference on Radar Meteorology*, Seattle, WA, August, 2003.

[10] M. W. Long, *Radar Reflectivity of Land and Sea*, 3rd ed. Artech House, 2001.

[11] D. A. Shnidman, "Comparison of low angle radar clutter models," *IEEE Trans. Aerosp. Electron. Syst.*, vol. 41(2), pp. 736–746, 2005.

[12] S. M. Kay, *Fundamentals of Statistical Signal Processing - Volume I: Estimation Theory*. New Jersey: Prentice-Hall, 1993.

[13] S. Julier, J. Uhlmann, and H. F. Durrant-White, "A new method for nonlinear transformation of means and covariances in filters and estimators," *IEEE Trans. Automat. Contr.*, vol. 45, pp. 477–482, 2000.

[14] B. Ristic, S. Arulampalam, and N. Gordon, *Beyond the Kalman Filter, Particle Filters for Tracking Applications*. Boston: Artech House, 2004.

[15] H. L. van Trees, *Detection, Estimation and Modulation Theory*. New York: John Wiley & Sons, 1968.

[16] P. Tichavský, C. H. Muravchik, and A. Nehorai, "Posterior Cramér-Rao bounds for discrete-time nonlinear filtering," *IEEE Trans. Signal Processing*, vol. 46 (5), pp. 1386–1396, 1998.

[17] *User's Manual for Advanced Refractive Effect Prediction System*, 3rd ed., Space and Naval Warfare Systems Center, Atmospheric Propagation Branch, San Diego, CA, April 2005. [Online]. Available: http://www.spawar.navy.mil/sti/publications.

[18] A. E. Barrios, "A terrain parabolic equation model for propagation in the troposphere," *IEEE Trans. Antennas Propagat.*, vol. 42 (1), pp. 90–98, 1994.

[19] J. P. Reilly and G. D. Dockery, "Influence of evaporation ducts on radar sea return," *IEE Proc. Radar and Signal Processing*, vol. 137 (F–2), pp. 80–88, 1990.